

Ground-Based Velocity Track Display (GBVTD) Analysis of W-Band Doppler Radar Data in a Tornado near Stockton, Kansas, on 15 May 1999

ROBIN L. TANAMACHI AND HOWARD B. BLUESTEIN

School of Meteorology, University of Oklahoma, Norman, Oklahoma

WEN-CHAU LEE AND MICHAEL BELL

National Center for Atmospheric Research, Boulder, Colorado

ANDREW PAZMANY

ProSensing, Inc., Amherst, Massachusetts

(Manuscript received 5 August 2005, in final form 19 June 2006)

ABSTRACT

On 15 May 1999, a storm intercept team from the University of Oklahoma collected high-resolution, W-band Doppler radar data in a tornado near Stockton, Kansas. Thirty-five sector scans were obtained over a period of approximately 10 min, capturing the tornado life cycle from just after tornadogenesis to the decay stage. A low-reflectivity “eye”—whose diameter fluctuated during the period of observation—was present in the reflectivity scans. A ground-based velocity track display (GBVTD) analysis of the W-band Doppler radar data of the Stockton tornado was conducted; results and interpretations are presented and discussed. It was found from the analysis that the axisymmetric component of the azimuthal wind profile of the tornado was suggestive of a Burgers–Rott vortex during the most intense phase of the life cycle of the tornado. The temporal evolution of the axisymmetric components of azimuthal and radial wind, as well as the wavenumber-1, -2, and -3 angular harmonics of the azimuthal wind, are also presented. A quasi-stationary wavenumber-2 feature of the azimuthal wind was analyzed from 25 of the 35 scans. It is shown, via simulated radar data collection in an idealized Burgers–Rott vortex, that this wavenumber-2 feature may be caused by the translational distortion of the vortex during the radar scans. From the GBVTD analysis, it can be seen that the maximum azimuthally averaged azimuthal wind speed increased while the radius of maximum wind (RMW) decreased slightly during the intensification phase of the Stockton tornado. In addition, the maximum azimuthally averaged azimuthal wind speed, the RMW, and the circulation about the vortex center all decreased simultaneously as the tornado decayed.

1. Introduction

A tornado is characterized by short horizontal scale and rapid evolution. Deduction of the horizontal wind field in and around a tornado remains a formidable task. Detailed understanding of tornado vortex structure is critical for the improvement of safeguard mechanisms for life and property. Bluestein et al. (2003a) noted that “there are relatively few detailed studies of

the wind field in actual tornadoes,” as positioning a high-resolution velocity measurement system within close range of a tornado is intrinsically difficult and dangerous.

Prior to the availability of such systems, the wind field in a tornadic vortex was the subject of extensive numerical and simulation studies. Comprehensive summaries of the state of scientific understanding of tornado vortex structure have been furnished by Davies-Jones and Kessler (1974), Davies-Jones (1986), Lewellen (1976, 1993), Rotunno (1993), and Davies-Jones et al. (2001). The current prevailing consensus favors the conceptual model of a tornado vortex possessing a one-celled (Burgers 1948; Rott 1958) or two-celled structure

Corresponding author address: Robin Tanamachi, School of Meteorology, University of Oklahoma, 120 David L. Boren Blvd., Norman, OK 73072.

E-mail: rtanamachi@ou.edu

(Sullivan 1959), or multiple vortices (Ward 1972; Church et al. 1979). Numerical and laboratory models depict the existence each of these possible conceptual models of the wind fields in and around a tornado vortex, and how the airflow characteristics (e.g., swirl ratio; Church et al. 1979) influence the favored vortex configuration and transitions between them. However, owing to the relatively small number of tornadoes that have been sampled observationally, the distribution of these vortex configurations, how the velocity configuration varies with height (3D wind field), the substorm-scale conditions under which each vortex configuration is favored, and how each configuration evolves with time, are not known in great detail. This study was motivated by the desire to address these uncertainties.

The use of mobile Doppler radars (e.g., Wurman and Gill 2000; Bluestein et al. 2004b; Kramar et al. 2005) has furnished much insight regarding the wind fields in and around tornadoes. However, high-resolution radar data (such as that furnished by a W-band radar) collected in tornadoes are still relatively scarce. Additionally, single-Doppler velocity data are inherently limited in their usefulness, in that they only provide information on the radial component of motion relative to the location of the radar. Information about the azimuthal wind structure of a horizontally complex feature, such as a tornado, that can be gleaned from such data is necessarily incomplete.

A number of different methods have been developed to overcome these limitations and allow for retrieval of 2D or 3D wind fields. What follows is a list of several notable methods: Dual-Doppler wind retrieval (e.g., Boucher et al. 1965), velocity-azimuth display (VAD) analysis (Lhermitte and Atlas 1962; Browning and Wexler 1968), Tracking Reflectivity Echoes by Correlation (TREC; Rinehart and Garvey 1978; Tuttle and Gall 1999; Kramar et al. 2005), “pseudo” dual-Doppler retrieval from Doppler radar data collected from an airborne platform (Jorgensen et al. 1983, 1996), synthetic dual-Doppler retrieval (Bluestein and Hazen 1989), and variational pseudomultiple ground-based (rolling range-height indicator) mobile Doppler wind synthesis (Weiss et al. 2006). The velocity-track display (VTD) analysis technique (Lee et al. 1994), and its two sibling techniques, the extended velocity track display (EVT) technique (Roux and Marks 1996) and the ground-based velocity track display (GBVTD) analysis technique (Lee et al. 1999), are single-Doppler 2D and 3D wind field retrieval techniques designed specifically for application to nearly axisymmetric atmospheric vortices such as tropical cyclones and tornadoes. The latter technique figures prominently in the content of the following study.

The study described in this paper was motivated by the desire to ascertain detailed information about the horizontal wind field in the immediate vicinity of a tornado. A high-resolution, W-band radar dataset was obtained in a tornado that occurred near Stockton, Kansas, on 15 May 1999. This dataset (consisting of both reflectivity and velocity) was subjected to GBVTD analysis, furnishing an objectively inferred two-dimensional wind field in the tornado.

A meteorological overview of the tornado is provided in section 2. In section 3, the characteristics of the W-band Doppler radar data collected in the Stockton tornado are summarized. Section 4 details the GBVTD analysis of the radar data; results and interpretations are discussed in sections 5 and 6, respectively. A summary of the study and conclusions is presented in section 7.

2. The Stockton, Kansas, tornado of 15 May 1999

On 15 May 1999, during a University of Oklahoma (OU) School of Meteorology storm intercept mission, a University of Massachusetts 95-GHz (W-band) mobile Doppler radar collected high-resolution radar reflectivity and velocity data from several seconds after tornadogenesis until the end of the life of a tornado that occurred near the town of Stockton in northwest Kansas (hereafter “the Stockton tornado,” see Fig. 1).

The Stockton tornado occurred in an isolated thunderstorm that developed over Rooks County, Kansas, at around 1920 CDT. Surface outflow from nearby thunderstorms generated easterly surface flow of 9 m s^{-1} at a location 18 km south of Stockton (Bluestein and Pazmany 2000). Aloft, the 0000 UTC, 16 May initialization of the Eta model indicated that southwest-easterly winds of approximately 18 and 19 m s^{-1} were present at 500 and 300 hPa, respectively, resulting in a value of shear close to 25 m s^{-1} between the surface and 500 hPa. At the time of the Stockton tornado, the storm appeared as a somewhat linear reflectivity echo on the Hastings, Nebraska, Weather Surveillance Radar-1988 Doppler (WSR-88D; Fig. 2).

Tornadogenesis occurred around 1955:12 CDT. During the organizing stage of the life cycle of the tornado, which lasted approximately 2 min, the condensation funnel had a ragged appearance. The tornado exhibited a multiple-vortex structure over a period of about 75 s starting around 1955:30 CDT. The tornado then changed to a classic “funnel” shape that was maintained for the next 8 min (the mature stage). In the last 2 min (the decaying stage) of its life cycle, the condensation funnel became thinner and corkscrewlike in appearance, before dissipating altogether at 2006:07 CDT. In



FIG. 1. The UMass W-band radar collecting data in the Stockton, KS, tornado. The view is to the northwest, and the truck is facing east. (Photograph courtesy of H. Bluestein.)

general, no multiple vortices were visible during the mature or decaying stages of the life cycle of the Stockton tornado. The Stockton tornado received a rating of F1 on the Fujita scale (Fujita 1981) as a result of damage to farmstead outbuildings and fences (NCDC 1999). Corroboratively, some tree damage was observed by the storm intercept team. However, the tornado traversed a relatively rural area, and therefore the tornado had little opportunity to damage well-built structures.

3. W-Band Doppler radar data

The Doppler radar data used in this study were collected by a mobile, 3-mm wavelength, 95-GHz (W-band), pulsed Doppler radar built by the University of Massachusetts (UMass) Microwave Remote Sensing Laboratory (Bluestein et al. 1995; hereafter “the W-band radar”). The W-band radar antenna has a half-power beamwidth of 0.18° , and the transmitter has a selectable pulse length of 15 or 30 m. The W-band radar transmitter implements a polarization diversity pulse pair (PDPP) technique (Doviak and Sirmans 1973) that effectively increases its maximum unambiguous velocity from ± 8 to $\pm 79 \text{ m s}^{-1}$ (Pazmany et al. 1999). The W-band radar has been used in numerous severe weather intercept programs (Bluestein et al. 1995, 1997, 2003a,b, 2004b; Pazmany et al. 1999; Bluestein and Pazmany 2000), and has also been used to collect data on other nonsevere meteorological phenomena such as dust devils (Bluestein et al. 2004a) and drylines (Weiss et al. 2006).

The W-band radar collected 35 high-resolution radar reflectivity and velocity scans in the Stockton tornado (Fig. 1). The first scan was collected at 1956:19 CDT, and the final scan at 2006:07 CDT. The time interval between scans was approximately 15 s, except for an interval of approximately 1 min (2001:55–2003:01 CDT) in which no scans were collected. The pulse length of the W-band radar was set to 30 m. The W-band radar was stationary throughout the collection period, during which the distance to the tornado, which moved toward the north-northwest, increased from 4.5 to 6.8 km (Fig. 3).

Significant changes in the structure of the Stockton tornado at various stages of its life cycle could be inferred from the radar data. Throughout the duration of the deployment, the tornado was characterized by one or more annuli of relatively high reflectivity, and was connected to the parent storm by a “thin band” of high reflectivity (described as an “umbilical cord” by Bluestein and Pazmany 2000) that was likely a rain curtain (Fig. 4). In the first 11 scans (covering the time interval from 1956:19 to 1958:26 CDT), the tornado was characterized by an annulus of relatively high reflectivity ($4\text{--}8 \text{ dBZ}_e$) around its center, and possibly a second annulus of moderate reflectivity (-10 to -5 dBZ_e) surrounding the inner high-reflectivity annulus (Fig. 4a). In the 12 scans, covering the time interval from 2000:55 to 2005:03 CDT, the tornado was characterized by a double annulus of relatively high reflectivity (-5 to -1 dBZ_e ; Fig. 1b). During the time interval between these two groups of scans, the reflectivity structure of the tornado underwent a transition that can be described as

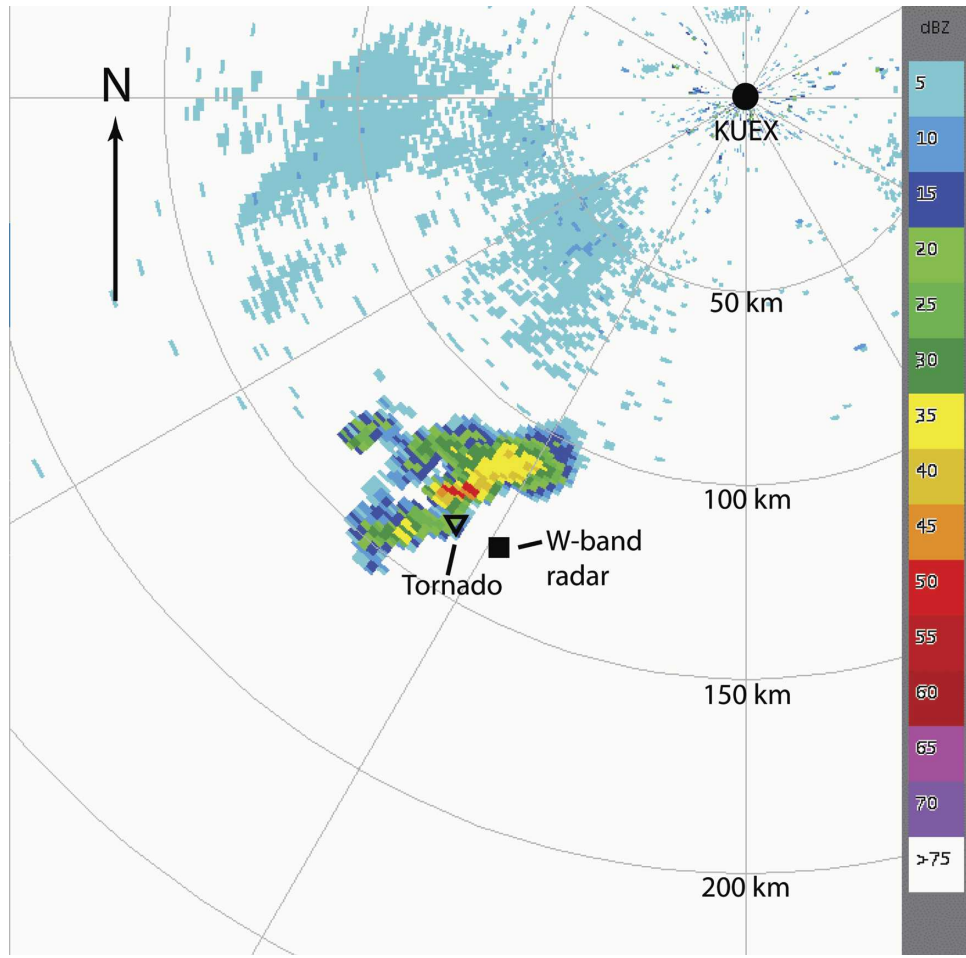


FIG. 2. WSR-88D reflectivity image of the storm that produced the Stockton tornado, taken at 1959 CDT by the WSR-88D located at Hastings, NE (KUEX). The range rings are spaced at 50-km intervals, and the azimuthal spacing is 30°. The black square indicates the approximate location of the UMass W-band radar; the inverted triangle indicates the approximate location of the tornado. The motion of the storm was toward the northeast.

“unraveling”: high-reflectivity filaments departed the inner high-reflectivity annulus, moved radially outward away from the center of the vortex, and formed a second, outer high-reflectivity annulus (Fig. 5).

The low-reflectivity “eye” in the center of the tornado, probably formed by the centrifuging of scatterers outward from the vortex center at, above, and below (assuming scatterer lofting) the level of the radar scan (Dowell et al. 2005), also exhibited significant variations in reflectivity structure throughout the course of the data collection. The eye underwent several “pulses” in which its width, as measured by the diametric distance between maximum negative gradients of reflectivity near the vortex center, increased and decreased in an arrhythmic fashion (Fig. 6).

During the data collection in the Stockton tornado, the Ford F350 pickup truck upon which the W-band

radar was mounted was not exactly level with respect to the level ground. As a result, the elevation angle measurements taken with the data were measured relative to the plane of the truck bed and not that of the level ground. The angle of the truck bed relative to the plane of the level ground along the “line of sight” between the truck and the tornado was not accurately known, but has been estimated to be $1.1^\circ \pm 0.3^\circ$ based upon photogrammetric analysis (described below). (In later seasons, hydraulic levelers were installed on the vehicle, enabling the radar to operate from a level truck bed and record accurate elevation angles.)

Additionally, the boresighted video camera installed on the radar dish, which is used by the radar operator to aim the radar beam, provided video feed to the radar operator, but this video feed was not recorded because the video cassette recorder malfunctioned. The radar

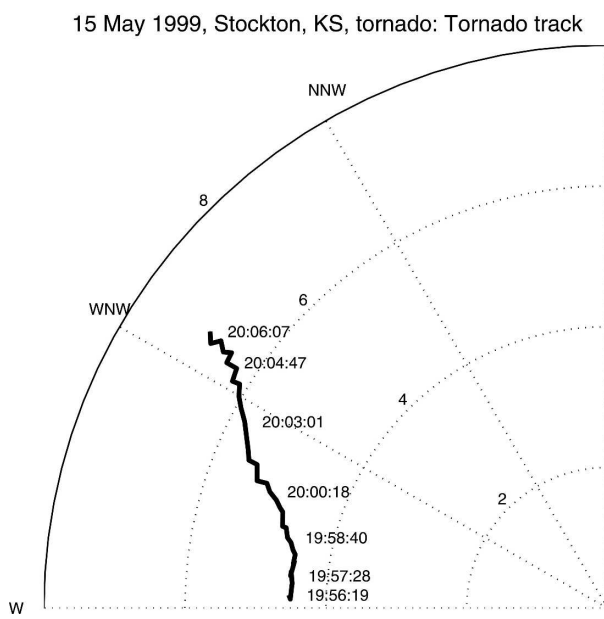


FIG. 3. Track of the Stockton tornado (based upon the location of the Doppler radar-measured velocity couplet) relative to the W-band radar, in polar coordinates. The W-band radar was located at the origin. Range rings are in km, times are in CDT (UTC – 5 h). The wiggles in the Doppler radar-derived tornado track were mainly an artifact of hysteresis of the radar antenna scanning mechanism (Bluestein et al. 2004a).

operator indicated that he attempted to aim the radar beam approximately halfway between the cloud base and the ground as seen in the video feed.

A continuous, time-stamped video recording was obtained of the W-band radar deployment and the tornado from a location approximately 30 m from the W-band radar deployment site. A photogrammetric analysis of still 35-mm slides (e.g., Fig. 1) that were matched to frames in the video, yielded an estimated scan height of 90 ± 20 m at a range of 4.5 km from the radar truck, and 125 ± 30 m at a range of 6.2 km (Fig. 7). These estimated heights correspond to an estimated radar elevation angle (with respect to the ground) of $1.1^\circ \pm 0.3^\circ$. The plane of the radar scan can therefore be assumed to be quasi-horizontal and the vertical component of motion contained within the measured along-beam component of the Doppler velocity is insignificant in comparison with the horizontal component.

4. GBVTD analysis procedure

The quasi-axisymmetric structure of the Stockton tornado at the level of the radar scan made the collected W-band radar dataset a prime candidate for application of GBVTD analysis. The reader is referred to Lee et al. (1999) and Bluestein et al. (2003b) for dis-

cussions of the GBVTD analysis technique and its application to another case in which high-resolution W-band radar data was collected in a tornado, respectively. The purpose of applying GBVTD analysis to this radar dataset was twofold: 1) to compare this case with a previous, similar case (the Bassett, Nebraska, tornado of 5 June 1999; detailed in Bluestein et al. 2003b), and 2) to ascertain new information about the structure of a tornado and its variations with time. The GBVTD analysis technique has been applied to radar data in order to ascertain information about the kinematic structure of tropical cyclones (Lee et al. 2000), in addition to tornadic vortices (Bluestein et al. 2003b; and the Mulhall, Oklahoma, tornado of 3 May 1999, discussed in Lee and Wurman 2005).

Some preprocessing of the W-band radar data was required in order to facilitate the application of the GBVTD analysis technique. The low-reflectivity eye often contained relatively noisy velocity data because there were relatively few scatterers located within. The GBVTD analysis, particularly the simplex center-seeking algorithm that is used, is somewhat sensitive to erroneous Doppler velocity data. To reduce the effects of such data on the GBVTD analysis, a reflectivity threshold was applied to the velocity data, using National Center for Atmospheric Research (NCAR) Solo-II radar data processing software (Oye et al. 1995). Any velocity data point associated with a reflectivity data point recorded as -18 dBZ_c or less was ignored; the velocity data from such points was considered suspect. A few additional velocity data points that were subjectively judged to be “suspect” (i.e., recorded rays in which the radar beam seemed to be blocked by a utility pole or other stationary obstruction) were also manually removed.

Successful application of the GBVTD technique requires that the aspect ratio between the radius of the tornado and the distance from the radar to the tornado not be excessively large (i.e., that the vortex not be located so close to the radar that the Doppler signature of the tornado becomes too distorted for accurate analysis; Wood and Brown 1992, 1997). The characteristics of the W-band radar dataset collected in the Stockton tornado satisfied the requirement that the aspect ratio was small, and that the data locations in radial and azimuthal space could be approximated as a Cartesian grid (Lee et al. 1999; Bluestein et al. 2003b).

Analysis of the 15 June 1999 Stockton tornado radar dataset using the GBVTD technique involved three main procedures:

- 1) The reflectivity and velocity data from each of the 35 sector scans were objectively analyzed, using a

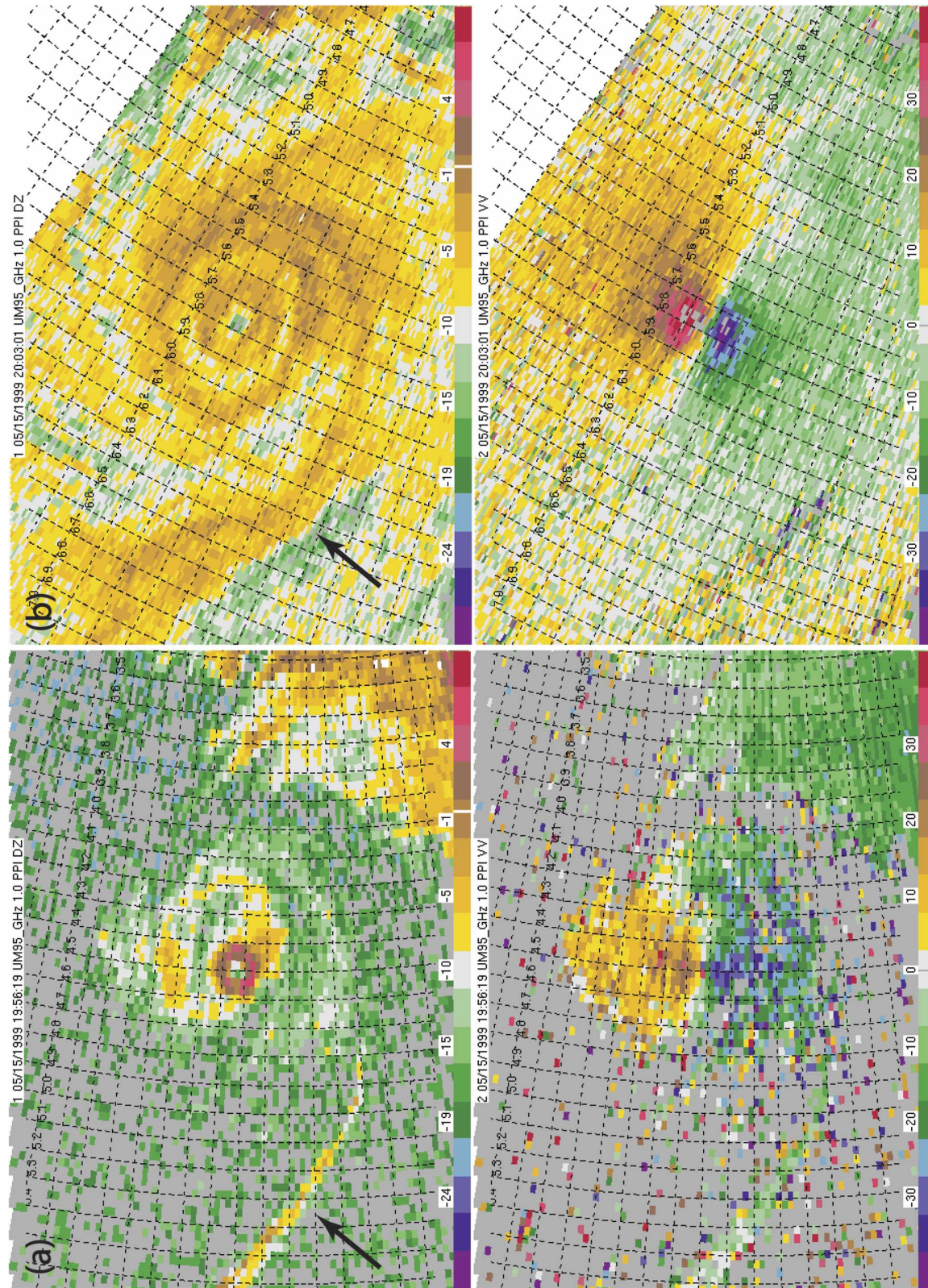


FIG. 4. (top) W-band reflectivity in dBZ_e and (bottom) Doppler velocity (m s^{-1}) in the Stockton tornado at (a) 1956:19 and (b) 2003:01 CDT. The azimuthal grid spacing is 1° and the radial grid spacing is 0.1 km. The black arrows indicate the location of the thin band of relatively high reflectivity connecting the vortex to the parent storm. The orientation of north is toward the top of the page.

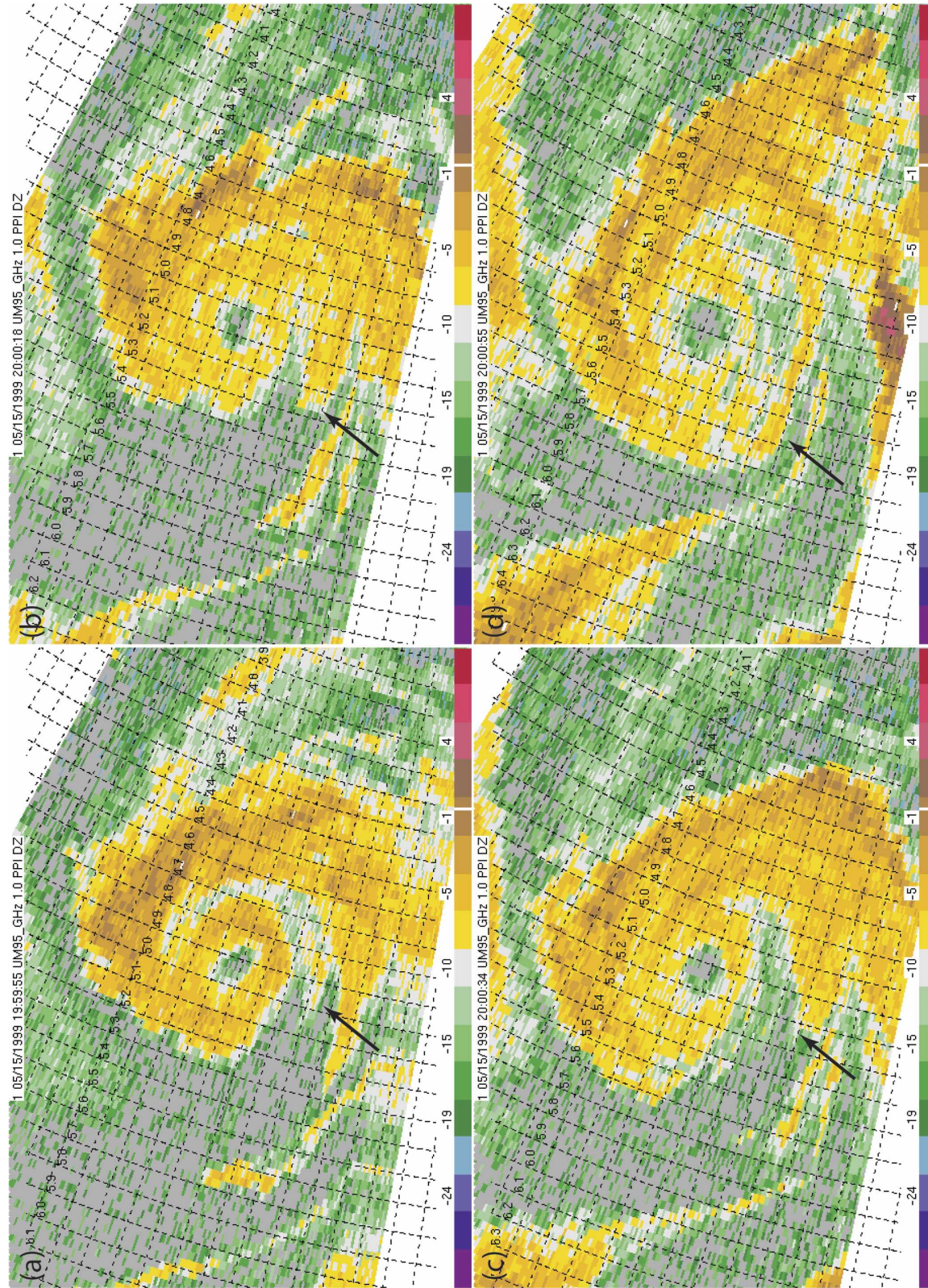


FIG. 5. Sequence of W-band reflectivity images from (a) 195955, (b) 200018, (c) 200034, and (d) 200034 CDT, showing the formation of the outer high-reflectivity annulus from the untraveling of an inner one (indicated by arrows). Note also the temporal continuity of the thin band of high reflectivity at right connecting the vortex to its parent storm. The azimuthal grid spacing is 1° and the radial grid spacing is 0.1 km. The orientation of north is toward the top of the page.

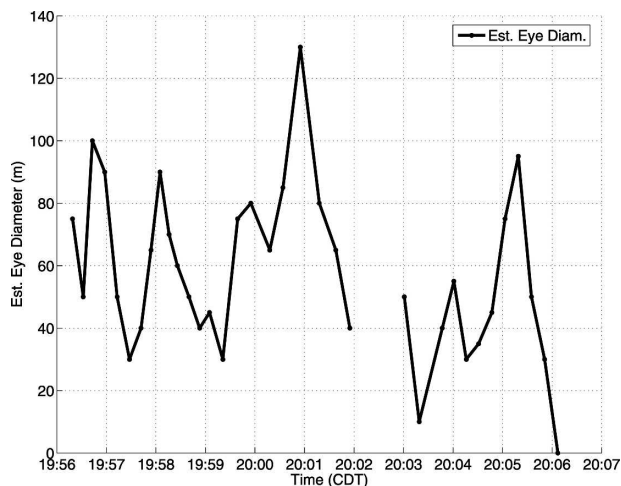


FIG. 6. Estimated diameter (m) of the low-reflectivity eye of the Stockton tornado as a function of time.

bilinear interpolation scheme (Mohr et al. 1986), from their recorded plan position indicator (PPI) grid in radar-centered polar coordinates (degrees and kilometers) to a constant altitude PPI (CAPPI) Cartesian coordinate grid with a grid spacing of 20 m. (The change in scan level height with distance, with respect to the ground, over the 150-m diameter of the tornado, which was approximately 4 m, was neglected.) The 20-m grid spacing was selected as a compromise between the radial resolution of the W-band radar (30 m) and its azimuthal resolution (15–20 m) at the range of the Stockton tornado (4.5–6.2 km).

- 2) The CAPPI grid point nearest the center of the tornado vortex was computed using the simplex vortex center-seeking algorithm of Lee and Marks (2000). This objectively determined vortex center was regarded with a high degree of confidence owing to the results of a sensitivity study (not shown) after that described in Bluestein et al. (2003b), which indicated that a vortex center displacement of two grid points or more would likely produce a prominent, spurious wavenumber-1 component.
- 3) The winds around the vortex center (determined in the previous step) were computed using the GBVTD analysis technique.

In the final procedure, the radar data were also transferred into a vortex-centered coordinate system, and the azimuthal winds were decomposed into azimuthally averaged wavenumber-0, -1, -2, and -3 angular harmonic components, as well as wavenumber-0 radial wind components, in 14 concentric annuli of 20-m thickness around the vortex center.

5. Results

The application of the GBVTD technique to the data collected by the UMass W-band radar yielded a set of GBVTD analyses of the vortex-centered two-dimensional wind field output for all 35 sector scans. Azimuthally averaged radial profiles of azimuthal and radial wind were used to calculate azimuthally averaged horizontal divergence and vertical vorticity. Azimuthally averaged values of reflectivity were also computed.

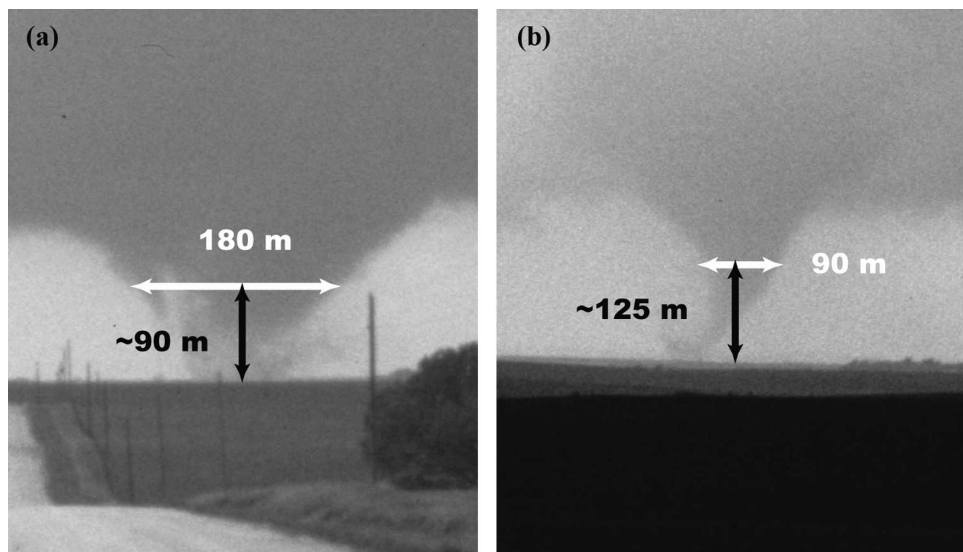


FIG. 7. Photogrammetric analyses of still photographs, obtained using a camera with a known focal length, that were matched to video frames (not shown). (Photographs courtesy of H. Bluestein.)

Examples of these analyses that are representative of different stages in the life cycle of the tornado are shown in Fig. 8. In general, the azimuthally averaged azimuthal velocity varied with radius like a Burgers-Rott vortex (BRV; Burgers 1948; Rott 1958), a version of the Rankine vortex in which the transition from the solid-body rotation in the inner radii to the potential flow at outer radii is smooth, rather than sharp or cusp-like. The maximum GBVTD-analyzed azimuthally averaged azimuthal wind was 45 m s^{-1} , which occurred at 2003:01 CDT. While this velocity is in the F2 range, it does not necessarily contradict the F1 rating assigned by NCDC to the Stockton tornado, because the radar data were collected at an altitude on the order of 100 m AGL. In general, the circulation increased with radius outward from the center of the vortex. The vorticity near the vortex center was approximately 2 s^{-1} , which is reasonable for a tornado.

To evaluate the quality of the GBVTD-analyzed azimuthally averaged azimuthal (radial) velocities, these velocities were compared to the Doppler velocities measured at a ring of constant radius from the radar (beam of constant azimuth) passing through the center of the tornado (e.g., Fig. 9). When the inherent noisiness of the radar data was taken into account, the sets of curves showed good agreement, and provided confidence in the results of the GBVTD analysis.

The intensity of the tornado, as measured by the maximum azimuthally averaged azimuthal wind speed, reached a peak of 45 m s^{-1} in the scan taken at 2003:01 CDT (Fig. 8e). At this time, the radial profile of azimuthally averaged azimuthal velocity for this scan bore a strong resemblance to a BRV. Manual fitting of a BRV profile (e.g., Davies-Jones 1986) to the maximum wind value and radius of maximum wind (RMW) only (45.0 m s^{-1} at 70 m) yields the agreeable profile shown in Fig. 10b. The profile underestimates the velocities beyond the RMW, indicating that perhaps the circulation is being underestimated in the BRV model.

A number of prominent features emerged from the time-averaged radial profiles of azimuthal and radial velocity, vorticity, divergence, and reflectivity during the time interval in which the tornado was approaching its peak intensity (1958:40–2003:01 CDT; Fig. 11). First, the RMW was located outside of the radius of maximum reflectivity (RMR), indicating that the highest velocities were located outside of the range ring with the greatest numbers of scatterers. Bluestein et al. (2004a) noted the same pattern in some W-band radar scans of dust devils in Texas, and hypothesized that it resulted from small particles being concentrated in the center of the vortex as a result of a frictionally induced surface-layer inflow. Second, the radial profile of azimuthally

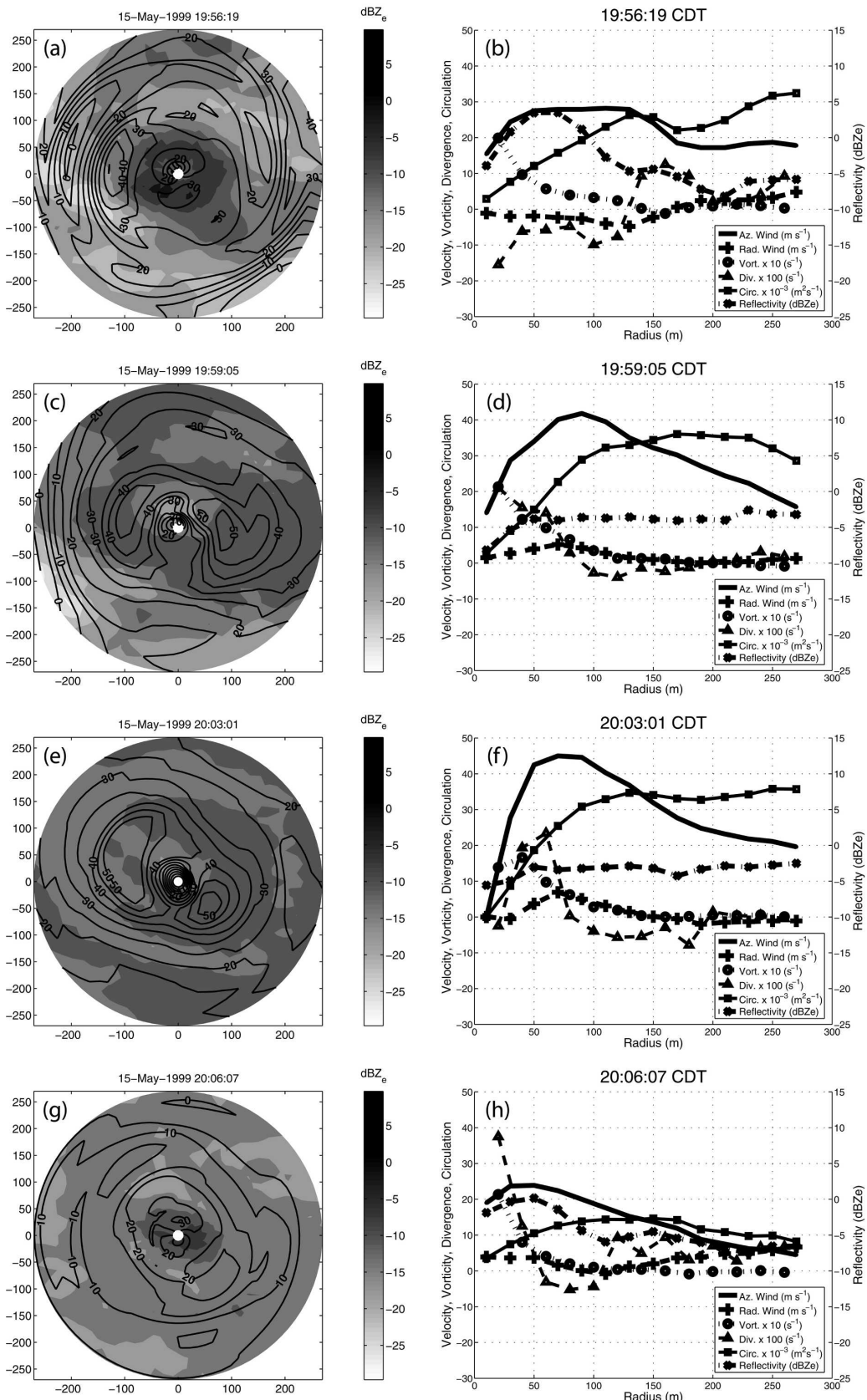
averaged radial velocity in the vortex at the level of the radar scan resembled that of a two-celled vortex (Sullivan 1959), although this structure cannot be definitively diagnosed via GBVTD analysis owing to uncertainties in the analyzed radial velocity, particularly at very small radii. Assuming that the two-celled vortex model was applicable and mass continuity was valid at the level of the radar scan, divergence (and possibly sinking motion aloft) was indicated between 30 and 140 m from the vortex center (a span encompassing the RMW), while convergence (and possibly rising motion aloft) was indicated between 140 and 260 m (well outside of the RMW). Dowell et al. (2005) assert that the velocities of centrifuged scatterers within a tornado may not be indicative of actual wind speeds inside of the tornado; however, this potential source of radial velocity (and hence, divergence) measurement error applies mainly to Doppler radar scans containing significant quantities of large scatterers, which were probably not present at the level of the radar scan (90–150 m AGL) in the Stockton tornado, except during intermittent periods. Third, the time-averaged radial profile of azimuthally averaged azimuthal wind again resembles a BRV.

After the scan in which the tornado reached its peak intensity (2003:01 CDT), the azimuthally averaged azimuthal wind quickly decreased over the next 3 min as the tornado dissipated.

6. Interpretation of the data

Figure 12 (Fig. 13) depicts the evolution of the azimuthally averaged azimuthal wind (circulation) structure as a function of time and radius. The maximum azimuthally averaged (wavenumber-0) component of the azimuthal wind increased in magnitude as the tornado progressed through its life cycle, and displayed good temporal continuity until the tornado began to decay around 2004:00 CDT. The circulation around the tornado increased from approximately $5000 \text{ m}^2 \text{s}^{-1}$ at the innermost analyzed radii to between 30 000 and 45 000 $\text{m}^2 \text{s}^{-1}$ at outermost analyzed radii when the tornado was in its mature stage. The decay phase of the Stockton tornado's life cycle is indicated both by a decrease in the maximum azimuthally averaged azimuthal wind and a decrease in circulation of the wavenumber-0 component of the azimuthal wind at all radii (Fig. 13).

The azimuthally averaged radial wind component of the tornado displayed a temporally coherent period of maximum velocity ($6\text{--}10 \text{ m s}^{-1}$ away from the vortex center) at roughly the same radii (60–120 m) and times (1958:40–2003:01 CDT) that the tornado was approaching its peak intensity (Fig. 14). Inflow into the tornado,



manifest as outbound velocities at the height of the scan at these radii and times, is consistent with the two-celled vortex model; however, as noted previously, a two-celled structure cannot be definitively diagnosed using this analysis. The GBVTD-analyzed values of azimuthally averaged radial velocity at radii less than 40 m should be considered particularly suspect because relatively few velocity data points contributed to the GBVTD analysis.

The GBVTD analyses also yielded azimuthally averaged radial profiles of higher-order angular harmonics of the azimuthal wind (wavenumbers-1, -2, and -3). All three of these components (not shown) display poor temporal continuity and are of little value for interpretation. However, a relatively strong wavenumber-2 component of azimuthal velocity, manifest as two quasi-diametrically opposed “lobes” of relatively high values of analyzed azimuthal velocity (e.g., Figs. 8c,e), was visibly present in 25 of the 35 analyses, with a wavenumber-2 magnitude of or exceeding 5 m s^{-1} .

Previous GBVTD analyses of radar data collected in tornadoes also exhibited a prominent wavenumber-2 component (Bluestein et al. 2003b; Lee and Wurman 2005). The reason for this feature is not definitively determined. It has been suggested that the wavenumber-2 component may be an artifact of the GBVTD analysis, or may in fact be a physical feature associated with tornadoes (Bluestein et al. 2003b). The orientation of the wavenumber-2 feature does not appear to be correlated with the direction of the radar beam, nor does it exhibit continuity in magnitude or orientation from scan to scan. It is also unlikely that the wavenumber-2 feature is the result of aliasing from higher-order harmonics (wavenumber-4, -6, etc.) owing to the relatively small contribution to the total azimuthal velocity component from the latter (Fig. 15).

A possible physical explanation for the wavenumber-2 feature is that it is a result of elliptical asymmetry of the vortex caused by translational and frictional effects (Shapiro 1983). Lee et al. (2005) hypothesized that a wavenumber-2 vortex Rossby wave (e.g., Montgomery and Kallenbach 1997) may actually be present in

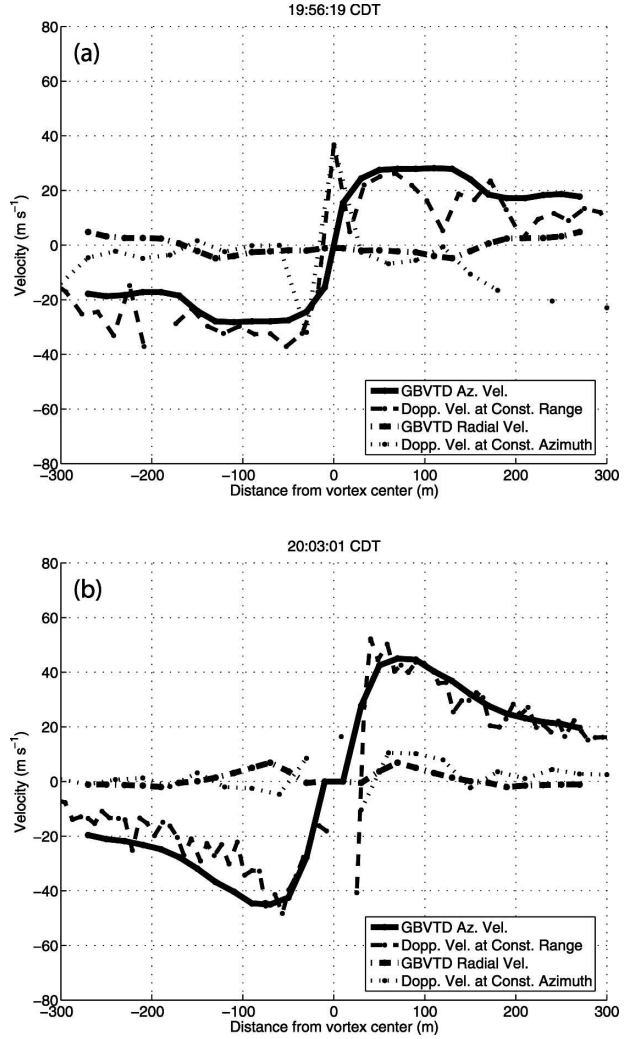


FIG. 9. GBVTD-analyzed wavenumber-0 (axisymmetric) azimuthal (solid line) and radial (dot-dashed line) velocities, and Doppler-measured along-beam velocities measured at constant range from the radar through tornado vortex (dashed line) and along the radial passing through the center of the tornado vortex (dotted line). The GBVTD-analyzed azimuthal velocities are portrayed as negative on the left-hand side for ease of comparison with the Doppler-measured velocities.

←

FIG. 8. (left) Reflectivity (filled gray contours with intervals of 5 dBZ_c) and GBVTD-analyzed azimuthal velocity (sum of wavenumbers 0–3, in contour intervals of 10 m s^{-1}). The direction of the radar beam is indicated by the arrow. (right) Radial profile of GBVTD-analyzed azimuthally averaged azimuthal velocity (m s^{-1}), radial velocity (m s^{-1}), vorticity ($\times 10 \text{ s}^{-1}$), divergence ($\times 100 \text{ s}^{-1}$), circulation ($\times 10^{-3} \text{ m}^2 \text{s}^{-1}$), and reflectivity (dBZ_c). Positive radial velocity indicates flow away from the tornado vortex center. These analyses were performed for the W-band radar scans collected at (a), (b) 1956:19 CDT, just after tornadogenesis; (c), (d) 1959:05 CDT, as the intensity of the tornado increased; (e), (f) 2003:01 CDT, when the tornado attained its peak intensity; and (g), (h) 2006:07 CDT, when the tornado dissipated.

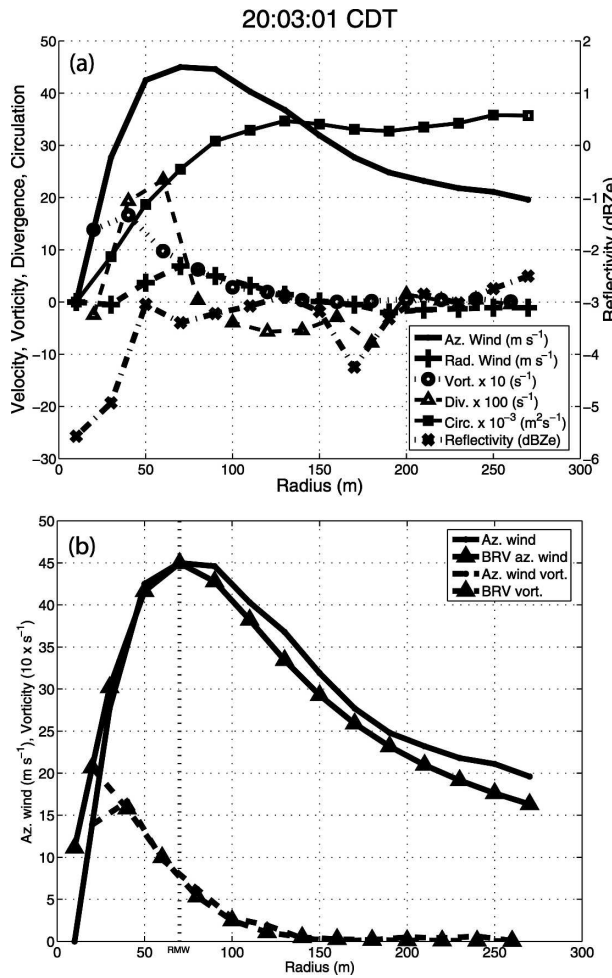


FIG. 10. (a) Radial profile of GBVTD-analyzed azimuthally averaged azimuthal velocity (m s^{-1}), radial velocity (m s^{-1}), vorticity ($\times 10 \text{ s}^{-1}$), divergence ($\times 100 \text{ s}^{-1}$), circulation ($\times 10^{-3} \text{ m}^2 \text{s}^{-1}$), and reflectivity (dBZ_e) at 2003:01 CDT, when the tornado was at peak intensity. Positive radial velocity indicates flow away from the tornado vortex center. (b) Radial profile of GBVTD-analyzed azimuthally averaged azimuthal velocity from 2003:01 CDT (solid curve), the azimuthal velocity profile of a BRV with the same maximum velocity value and RMW (solid curve with triangular markers). The vorticity associated with each of the profiles (multiplied by a factor of 10 for clarity) is indicated by broken lines with corresponding symbols.

elliptically shaped atmospheric vortices, but one would expect the high-velocity lobes to revolve around the center of the tornado (Bluestein et al. 2003b), and this progression is not obvious in the analyses. The presence of a wavenumber-2 vortex Rossby wave would be impossible to verify without high-resolution *volumetric* radar data collected in close proximity to the vortex.

The authors believe that a likely explanation for the wavenumber-2 feature is that it is an artifact resulting from the motion of the tornado during the time interval over which a radar scan was collected. The motion of

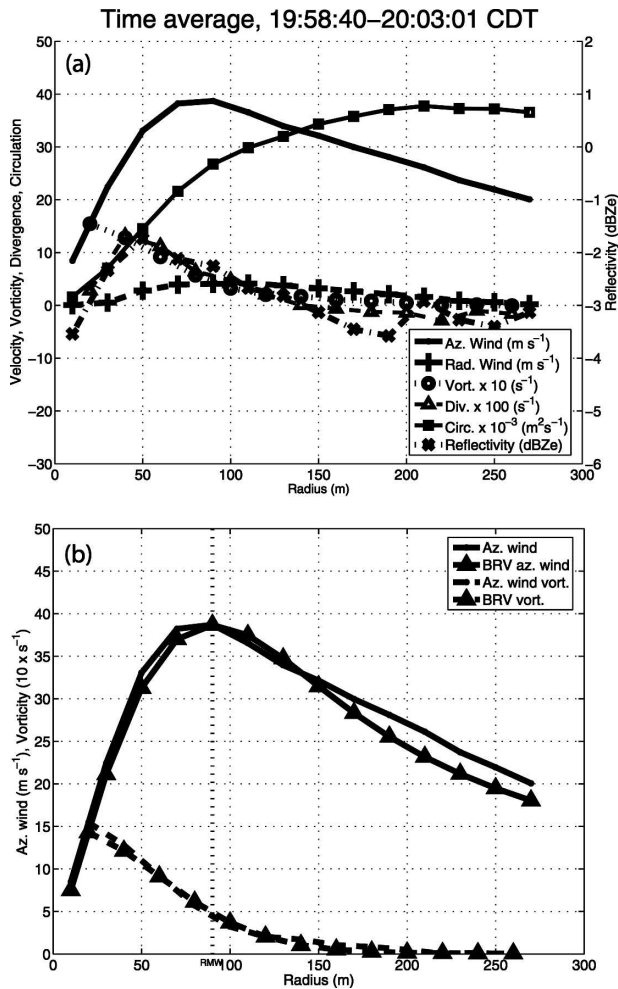


FIG. 11. Same as in Fig. 10, but for the time average over the interval 19:58:40–20:03:01 CDT (excluding the data gap from 2001:55 to 2003:01 CDT), when the tornado was approaching its peak intensity.

the vortex (approximately 7 m s^{-1} to the north-northwest) during the time interval required to collect the radar scan (approximately 10 s) is enough to distort the vortex into an ellipse. The distortion of the vortex causes a spurious wavenumber-2 feature in the resulting GBVTD analysis.

In idealized experiments, a BRV azimuthal velocity profile closely resembling that of a tornado was sought. Subjectively guessed values of circulation Γ ($45\ 000 \text{ m}^2 \text{s}^{-1}$), RMW (70 m), and azimuthal velocity at the RMW (80 m s^{-1}) were used. An idealized, cyclonic vortex with this velocity profile, centered at the point (0 and 5000 m), was generated. This vortex velocity field was “sampled” with a radial resolution of 10 m and an azimuthal resolution of 0.2° (mimicking somewhat the 30-m radial resolution and 0.18° beamwidth of the W-band radar) by a stationary “radar” located at the ori-

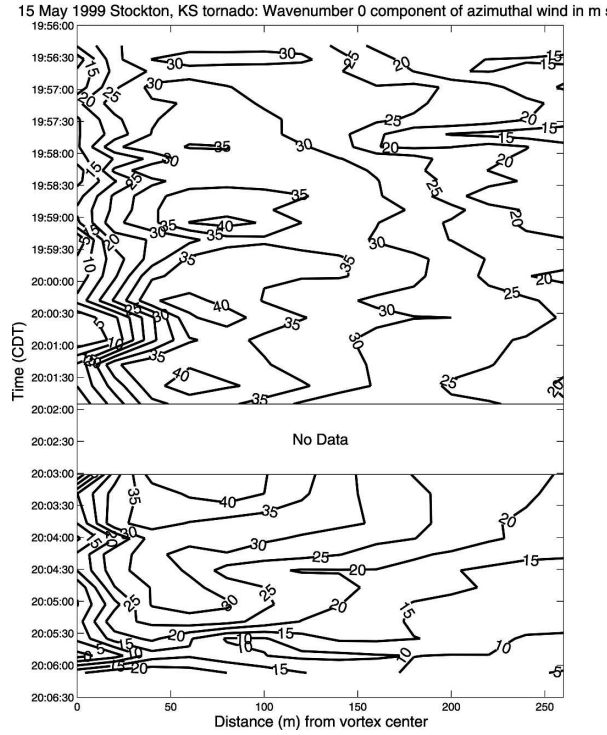


FIG. 12. Hovmoeller diagram of the azimuthally averaged (wavenumber-0) component of the azimuthal velocity as a function of radius in the Stockton tornado, as computed by the GBVTD analysis. The radius of the eye approached 60 m around 2001 CDT, resulting in the abnormally small velocities analyzed in the 20–40-m radius ring at that time. Minimum F0 tornado velocity is 35 m s⁻¹.

gin. The along-beam component of vortex velocity was calculated, and an instantaneous simulated Doppler velocity field (not shown) was generated.

This procedure was repeated, this time simulating the Doppler velocity field that would be generated by a Doppler radar scanning a horizontally translating BRV with the same velocity field. Doppler velocity scans were simulated for combinations of three different antenna rotation rates (+1°, +2°, and +4° s⁻¹), four vortex translation speeds (0, 5, 10, and 15 m s⁻¹), and eight different directions of motion (0°–315° in increments of 45°). The simulated Doppler velocity fields were then interpolated to a Cartesian grid with a resolution of 20 m, and subjected to VTD (Lee et al. 1999) analysis about the vortex center.

It was observed that a wavenumber-2 component (with varying degrees of prominence) was analyzed from most of these simulated Doppler radar scans (not shown). To see how well the simulation matched up with the analysis results, an additional simulation was conducted in which the simulated BRV closely mimicked the characteristics (RMW, maximum azimuthal

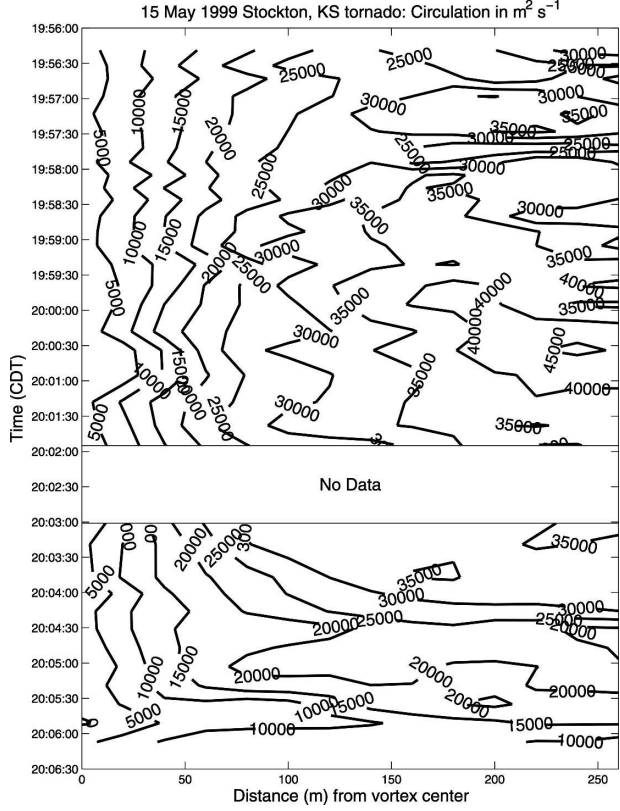


FIG. 13. Hovmoeller diagram of azimuthally averaged circulation as a function of radius in the Stockton tornado, computed from the GBVTD-analyzed, azimuthally averaged wavenumber-0 component of the azimuthal velocity.

velocity, position, and motion) of the tornado at 2003:01 CDT. The simulated radar data were generated using nearly the same “scanning” strategy (antenna rotation rate and direction) as that of the actual W-band radar. The resulting GBVTD analysis is shown in Fig. 16. This analysis features a prominent wavenumber-2 component with an amplitude of 5 m s⁻¹ (relative to wavenumber-0 component of 40 m s⁻¹) at a radius of 70 m from the center of the vortex. Although the orientation of the wavenumber-2 features differ, the structural similarities between Fig. 8e and Fig. 16 are remarkable. These results lead the authors to favor vortex transaction as an explanation of the wavenumber-2 feature.¹

A possible explanation for the poor temporal continuity in orientation of the wavenumber-2 feature is the presence of a vertically propagating wavenumber-2 feature (such as an inertial wave) within the tornado vor-

¹ Note added in proof: Results of subsequent work have not borne out this conclusion’s having the degree of importance implied here. The authors intend to detail pertinent findings in a future publication.

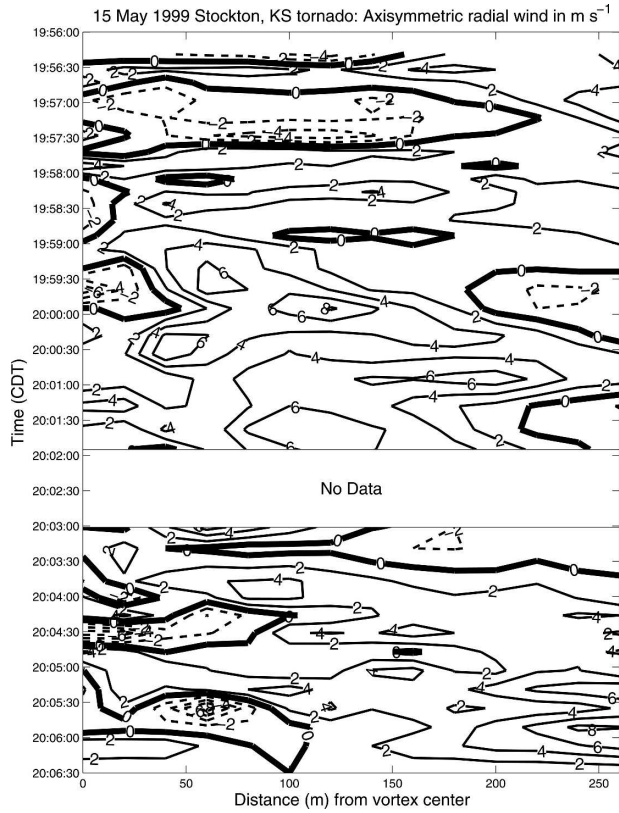


FIG. 14. Hovmoeller diagram of azimuthally averaged radial velocity as a function of radius in the Stockton tornado, as computed by the GBVTD analysis. Note the coherent interval of inflow between 60- and 120-m radius during the time interval 1958:40–2003:01 CDT. The analyzed values at 2004:31 CDT are highly suspect because the reflectivities in the vortex were relatively small over the entire GBVTD analysis domain.

tex structure. However, as with a vortex Rossby wave, such a feature would be impossible to resolve without rapidly collected, high-resolution, volumetric radar data. Another possible explanation is the alternating azimuthal direction of radar sweep that is responsible for the “wiggles” in the tornado track (Fig. 3). This apparent change in direction and speed of the tornado can, in turn, influence the results of the GBVTD analysis.

The observed vortex structure is complex, and any underlying physical wavenumber-2 asymmetry may be distorted by the above-mentioned artifacts. To further elucidate the physical vortex asymmetries, methods to compensate for distortion of the vortex and the motion of the radar antenna are currently under development.

A number of significant features of the evolution of the Stockton tornado became apparent when several time-dependent variables were plotted on the same axis (Fig. 17). First, the low-reflectivity eye width decreased as the tornado approached its peak intensity (as mea-

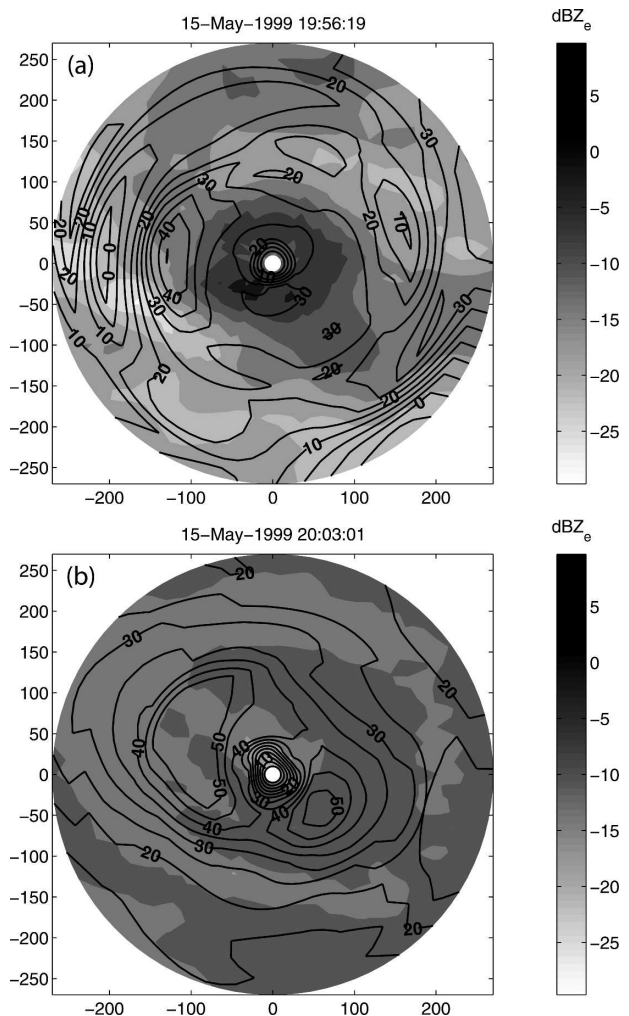


FIG. 15. (a), (b) Same GBVTD analyses depicted in Figs. 8a,e, respectively, but with wavenumber 4 also included. The direction of the radar beam is indicated by the black arrow. North is toward the top of the page.

sured by the maximum azimuthally averaged azimuthal wind) at 2003:01 CDT, and then increased again as the tornado decayed. This fluctuation in eye width could be indicative of increased lofting of small raindrops and low-density debris particles (such as grass and dust) near the RMW as the intensity of the tornado increased (D. Burgess 2004, personal communication). Dowell et al. (2005), using a quasi-3D simulation of an axisymmetric tornadic vortex, showed that relatively small particles (such as raindrops) can be concentrated near the core of the tornado in the surface inflow layer, and then transported upward by the central updraft. Other arrhythmic fluctuations in eye width could result from the intermittent ingestion by the tornado of large quantities of small particles, which were then lofted to the level of the radar scan (Bluestein et al. 2004a).

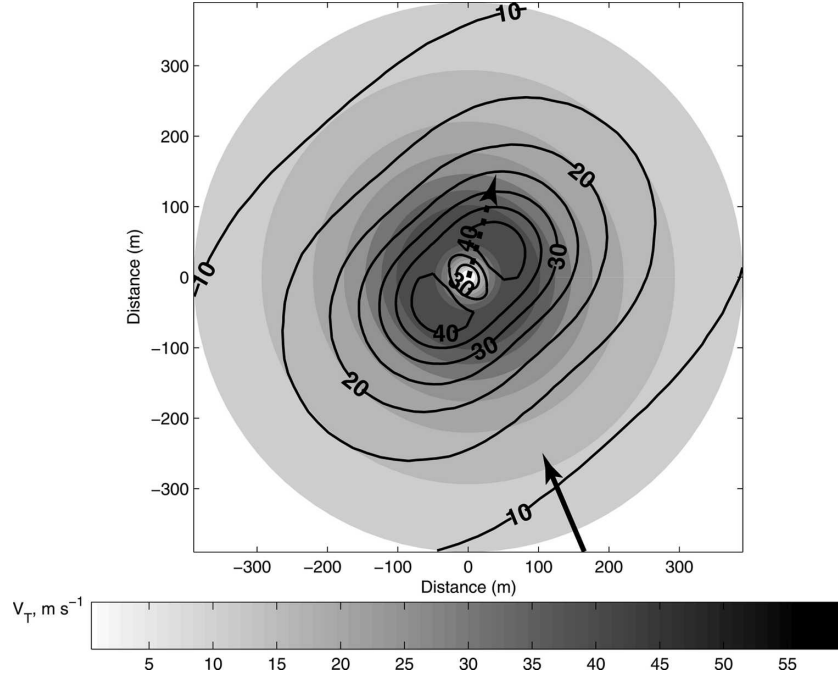


FIG. 16. GBVTD-analyzed azimuthal velocity fields (black contours in increments of 5 m s^{-1}), generated from simulated radar scans in which an idealized BRV translated at 11 m s^{-1} at an angle of 5° clockwise from north, a motion similar to the tornado observed at 2003:01 CDT. For comparison, the idealized BRV azimuthal velocity field (filled gray contours, scale at bottom) is also shown. The vector pointing from the radar to the simulated vortex center is indicated by the solid black arrow, and the direction of motion of the vortex by the dashed arrow.

Second, during the intensification period of the tornado (1958:40–2003:01 CDT), it can be seen that an increase in the maximum azimuthally averaged azimuthal wind at a relatively steady RMW resulted in an increase in circulation at the RMW. This manner of tornado intensification contrasts with that found by Bluestein et al. (2003b) in their GBVTD analysis of the 5 June 1999 Bassett, Nebraska, tornado (hereafter, “the Bassett tornado”). The RMW of the Bassett tornado decreased while the maximum azimuthally averaged azimuthal wind increased, and the circulation of the tornado at the RMW increased. This result suggests that more than one mode of tornado intensification exists.

Third, it can be seen that as the tornado decreased in intensity toward the end of its life cycle (after 2003:01 CDT), the RMW also generally decreased. This result is consistent with the visual appearance of the tornado; the visible condensation funnel appeared to narrow before dissipating. This behavior contrasts markedly with the decay mode found by Bluestein et al. (2003b) in the Bassett tornado. The Bassett tornado exhibited an increase in the RMW and a simultaneous decrease in maximum azimuthally averaged azimuthal wind. This

result suggests that more than one mode of tornado decay exists, a conclusion that is consistent with the two decay modes suggested by Davies-Jones et al. (2001).

7. Conclusions

Application of the GBVTD analysis technique provided insights on the horizontal wind field in the 15 May 1999 Stockton, Kansas, tornado, in which exceptionally high-quality W-band radar data were collected. From the GBVTD analysis, it can be inferred that the Stockton tornado wind field at the height of the radar scan resembled that of a Burgers–Rott vortex during the period in which the tornado approached its peak intensity (1958:40–2003:01 CDT).

It can be seen from the radar data that the width of the low-reflectivity “eye” in the center of the tornado vortex fluctuated from scan to scan. Of particular interest, the eye width decreased as the tornado approached its peak intensity at 2003:01 CDT. One might expect that the width of the eye would increase with increasing tornado intensity as a result of increased centrifuging of scatterers (Dowell et al. 2005). It is noted that the eye width decreased again as the tornado de-

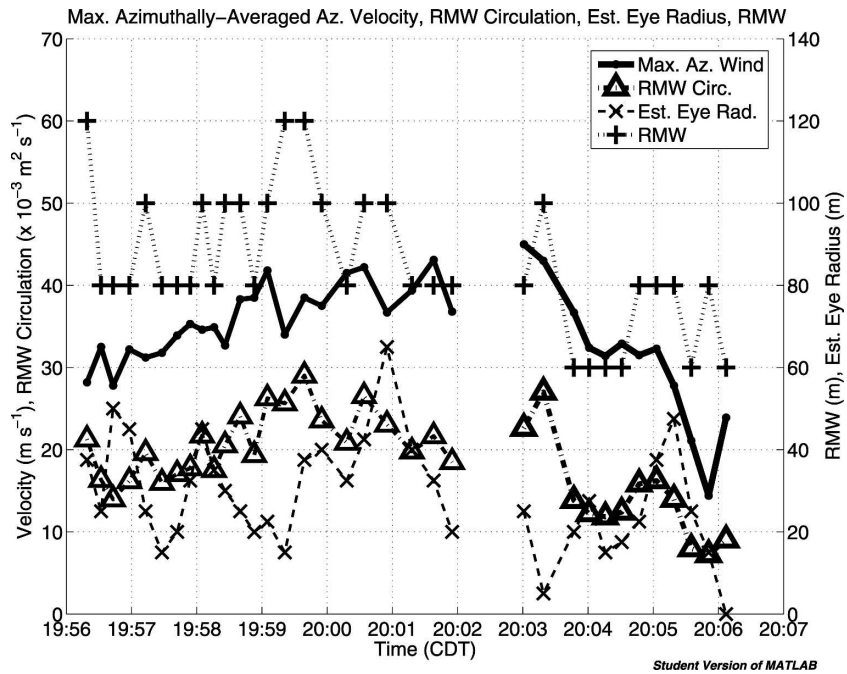


FIG. 17. Maximum azimuthally averaged azimuthal velocity, RMW, and estimated eye radius of the Stockton tornado as functions of time.

cayed. These fluctuations could be indicative of increased ingestion and lofting of light debris inside the tornado, up to the altitude of the radar scan, as the intensity of the tornado increased.

From a comparison of the GBVTD analyses of the Stockton tornado and the Bassett tornado (Bluestein et al. 2003b), it can be inferred that tornadoes exhibit two or more different modes of intensification and two or more different modes of decay. As the RMW remained relatively constant during the intensification phase of the Stockton tornado, with a few noticeable exceptions, the increase in RMW circulation resulted primarily from an increase of the maximum azimuthally averaged azimuthal velocity; the RMW circulation in the Bassett tornado increased as a result of an increase of the maximum azimuthally averaged velocity that occurred along with a simultaneous decrease of the RMW. The RMW circulation of the Stockton tornado decayed as a result of a simultaneous decrease of *both* the maximum azimuthally averaged azimuthal velocity and the RMW; the RMW circulation of the Bassett tornado decayed as a result of a decrease of the maximum azimuthally averaged azimuthal velocity, despite an increase of the RMW.

A significant wavenumber-2 component, with its amplitude at or exceeding 5 m s^{-1} , of the azimuthal wind was present in 25 out of 35 of the W-band sector scans. Similar wavenumber-2 features have been observed in previous studies in which the GBVTD analysis tech-

nique has been applied to mobile radar data collected in tornadoes. The presence of the wavenumber-2 feature in analyses of data collected by multiple radars (Lee and Wurman 2005; Bluestein et al. 2003b) suggests that the wavenumber-2 feature may have a physical basis. However, it was shown in this study that the wavenumber-2 feature may have resulted from the distortion of the vortex in the radar image caused by the vortex motion. Methods to compensate for this distortion in the radar data are being developed and will be the subject of future work.

Additional GBVTD analyses of mobile radar data collected in other tornadoes could provide a means of strengthening or disproving theories about tornado structure and evolution presented in this study and elsewhere. GBVTD analyses of data from radars with higher scan rates than the W-band radar could potentially clarify the source of the wavenumber-2 feature that has been repeatedly observed in mobile radar data collected in tornadoes. GBVTD analyses of data from radars that collect data at multiple-elevation angles simultaneously [e.g., the rapid-scan Doppler on Wheels (DOW5); Wurman and Randall 2001] and from dual-polarization radars (e.g., Lopez et al. 2004) could also potentially illuminate the structure of tornadoes.

Acknowledgments. This research was conducted as part of the first author's master's thesis project. S. P.

Nelson of the National Science Foundation (NSF) supported this research under NSF Grants ATM-9320672, ATM-9616730, and ATM-0241037, and supplements to NSF Grants ATM-9019821, ATM-9302379, and ATM-9612674. D. Dowell of the Cooperative Institute for Mesoscale Meteorological Studies at OU furnished a copy of his video recording of the Stockton tornado. M. Laufersweiler provided technology support. E. Rasmussen provided nowcasting support. M. I. Biggerstaff and A. Shapiro of OU, L. J. Wicker, D. Jorgensen, D. W. Burgess, and V. T. Wood of the National Severe Storms Laboratory, and C. C. Weiss of Texas Tech University provided discussion and assistance throughout the research process. The authors gratefully acknowledge three anonymous reviewers who helped us to greatly improve the clarity and quality of the manuscript.

REFERENCES

- Bluestein, H. B., and D. S. Hazen, 1989: Doppler-radar analysis of a tropical cyclone over land: Hurricane Alicia (1983) in Oklahoma. *Mon. Wea. Rev.*, **117**, 2594–2611.
- , and A. L. Pazmany, 2000: Observations of tornadoes and other convective phenomena with a mobile, 3-mm wavelength, Doppler radar: The spring 1999 field experiment. *Bull. Amer. Meteor. Soc.*, **81**, 2939–2951.
- , —, J. C. Galloway, and R. E. McIntosh, 1995: Studies of the substructure of severe convective storms using a mobile 3-mm-wavelength Doppler radar. *Bull. Amer. Meteor. Soc.*, **76**, 2155–2170.
- , S. G. Gaddy, D. C. Dowell, A. L. Pazmany, J. C. Galloway, R. E. McIntosh, and H. Stein, 1997: Doppler radar observations of substorm-scale vortices in a supercell. *Mon. Wea. Rev.*, **125**, 1046–1059.
- , C. C. Weiss, and A. L. Pazmany, 2003a: Mobile Doppler radar observations of a tornado in a supercell near Bassett, Nebraska, on 5 June 1999. Part I: Tornadogenesis. *Mon. Wea. Rev.*, **131**, 2954–2967.
- , W.-C. Lee, M. Bell, C. C. Weiss, and A. L. Pazmany, 2003b: Mobile Doppler radar observations of a tornado in a supercell near Bassett, Nebraska, on 5 June 1999. Part II: Tornado-vortex structure. *Mon. Wea. Rev.*, **131**, 2968–2984.
- , C. C. Weiss, and A. L. Pazmany, 2004a: Doppler radar observations of dust devils in Texas. *Mon. Wea. Rev.*, **132**, 209–224.
- , —, and —, 2004b: The vertical structure of a tornado near Happy, Texas, on 5 May 2002: High-resolution, mobile, W-band, Doppler radar observations. *Mon. Wea. Rev.*, **132**, 2325–2337.
- Boucher, R. J., R. Wexler, D. Atlas, and R. M. Lhermitte, 1965: Mesoscale structure revealed by Doppler radar. *J. Appl. Meteor.*, **4**, 590–597.
- Browning, K. A., and R. Wexler, 1968: The determination of kinematic properties of a wind field using Doppler radar. *J. Appl. Meteor.*, **7**, 105–113.
- Burgers, J. M., 1948: A mathematical model illustrating the theory of turbulence. *Adv. Appl. Mech.*, **1**, 197–199.
- Church, C. R., J. T. Snow, G. L. Baker, and E. M. Agee, 1979: Characteristics of tornado-like vortices as a function of swirl ratio: A laboratory investigation. *J. Atmos. Sci.*, **36**, 1755–1776.
- Davies-Jones, R., 1986: Tornado dynamics. *Thunderstorm Morphology and Dynamics*, 2d ed. E. Kessler, Ed., University of Oklahoma Press, 197–236.
- , and E. Kessler, 1974: Tornadoes. *Weather and Climate Modification*, W. N. Hess, Ed., Wiley and Sons, 552–595.
- , R. J. Trapp, and H. B. Bluestein, 2001: Tornadoes and tornadic storms. *Severe Convective Storms, Meteor. Monogr.*, No. 28, Amer. Meteor. Soc., 167–21.
- Doviak, R. J., and D. Sirmans, 1973: Doppler radar with polarization diversity. *J. Atmos. Sci.*, **30**, 737–738.
- Dowell, D. C., C. A. Alexander, J. Wurman, and L. J. Wicker, 2005: Centrifuging of hydrometeors and debris in tornadoes: Radar-reflectivity patterns and wind-measurement errors. *Mon. Wea. Rev.*, **133**, 1501–1524.
- Fujita, T. T., 1981: Tornadoes and downbursts in the context of generalized planetary scales. *J. Atmos. Sci.*, **38**, 1511–1534.
- Jorgensen, D. P., P. H. Hildebrand, and C. L. Frush, 1983: Feasibility test of an airborne pulse-Doppler meteorological radar. *J. Climate Appl. Meteor.*, **22**, 744–757.
- , T. Matejka, and J. D. DuGranrut, 1996: Multi-beam techniques for deriving wind fields from airborne Doppler radars. *J. Meteor. Atmos. Phys.*, **59**, 83–104.
- Kramar, M. R., H. B. Bluestein, A. L. Pazmany, and J. D. Tuttle, 2005: The “Owl Horn” radar signature in developing Southern Plains supercells. *Mon. Wea. Rev.*, **133**, 2608–2634.
- Lee, W. C., and F. D. Marks Jr., 2000: Tropical cyclone kinematic structure retrieved from single-Doppler radar observations. Part II: The GBVTD-simplex center-finding algorithm. *Mon. Wea. Rev.*, **128**, 1925–1936.
- , and J. Wurman, 2005: Diagnosis of 3D wind structure of the Mulhall, Oklahoma, tornado of 3 May 1999. *J. Atmos. Sci.*, **62**, 2373–2393.
- , F. D. Marks Jr., and R. E. Carbone, 1994: Velocity track display—A technique to extract real-time tropical cyclone circulations using a single airborne Doppler radar. *J. Atmos. Oceanic Technol.*, **11**, 337–356.
- , B. J.-D. Jou, P.-L. Chang, and S.-M. Deng, 1999: Tropical cyclone kinematic structure retrieved from single-Doppler radar observations. Part I: Doppler velocity patterns and the GBVTD technique. *Mon. Wea. Rev.*, **127**, 2419–2439.
- , —, —, and F. D. Marks Jr., 2000: Tropical cyclone kinematic structure retrieved from single-Doppler radar observations. Part III: Evolution and structures of Typhoon Alex. *Mon. Wea. Rev.*, **128**, 3982–4001.
- , P. Harasti, M. Bell, B. J.-D. Jou, and H.-H. Chang, 2005: Doppler velocity signatures of idealized elliptical vortices. *Terr. Atmos. Oceanic Sci.*, **17**, 429–446.
- Lewellen, W. S., 1976: Theoretical models of the tornado vortex. *Proceedings, Symposium on Tornadoes: Assessment of Knowledge and Implications for Man*, R. E. Peterson, Ed., Texas Tech University, 107–143.
- , 1993: Tornado vortex theory. *The Tornado: Its Structure, Dynamics, Prediction, and Hazards, Geophys. Monogr.*, Vol. 79, Amer. Geophys. Union, 19–39.
- Lhermitte, R. M., and D. Atlas, 1962: Precipitation motion by pulse Doppler radar. *Proc. Ninth Weather Radar Conf.*, Kansas City, MO, Amer. Meteor. Soc., 218–223.
- Lopez, F. J., A. L. Pazmany, H. B. Bluestein, M. R. Kramar, M. F. French, C. C. Weiss, and S. Frasier, 2004: Dual-polarization, X-band, mobile Doppler radar observations of hook echoes

- in supercells. Preprints, 22d Conf. on Severe Local Storms, Hyannis, MA, Amer. Meteor. Soc., CD-ROM, P11.7.
- Mohr, C. G., L. J. Miller, R. L. Vaughn, and H. W. Frank, 1986: Merger of mesoscale dataset into a common Cartesian format for efficient and systematic analysis. *J. Atmos. Oceanic Technol.*, **3**, 143–161.
- Montgomery, M. T., and R. J. Kallenbach, 1997: A theory for vortex Rossby-waves and its application to spiral bands and intensity changes in hurricanes. *Quart. J. Roy. Meteor. Soc.*, **123**, 435–465.
- NCDC, 1999: *Storm Data*. Vol. 37, No. 5, 372 pp.
- Oye, R. C., K. Mueller, and S. Smith, 1995: Software for radar translation, editing, and interpolation. Preprints, 27th Conf. on Radar Meteorology, Vail, CO, Amer. Meteor. Soc., 359–361.
- Pazmany, A. L., J. C. Galloway, J. B. Mead, I. Popstefanija, R. E. McIntosh, and H. B. Bluestein, 1999: Polarization diversity pulse-pair technique for millimeter-wave Doppler radar measurements of severe storm features. *J. Atmos. Oceanic Technol.*, **16**, 1900–1911.
- Rinehart, R. E., and E. T. Garvey, 1978: Three-dimensional storm motion detection by conventional weather radar. *Nature*, **273**, 287–289.
- Rott, N., 1958: On the viscous core of a line vortex. *Z. Angew. Math. Phys.*, **9**, 543–553.
- Rotunno, R., 1993: Supercell thunderstorm modeling and theory. *The Tornado: Its Structure, Dynamics, Prediction, and Hazards*, Geophys. Monogr., Vol. 79, Amer. Geophys. Union, 57–73.
- Roux, F., and F. D. Marks Jr., 1996: Extended Velocity Track Display (EVTD): An improved processing method for Doppler radar observations of tropical cyclones. *J. Atmos. Oceanic Technol.*, **13**, 875–899.
- Shapiro, L. J., 1983: The asymmetric boundary flow layer under a translating hurricane. *J. Atmos. Sci.*, **40**, 1984–1998.
- Sullivan, R. D., 1959: A two-cell vortex solution of the Navier-Stokes equations. *J. Aerospace Sci.*, **26**, 767–768.
- Tuttle, J., and R. Gall, 1999: A single-radar technique for estimating the winds in tropical cyclones. *Bull. Amer. Meteor. Soc.*, **80**, 653–668.
- Ward, N. B., 1972: The exploration of certain features of tornado dynamics using a laboratory model. *J. Atmos. Sci.*, **29**, 1194–1204.
- Weiss, C. C., H. B. Bluestein, and A. L. Pazmany, 2006: Finescale radar observations of the 22 May 2002 dryline during the International H₂O Project (IHOP). *Mon. Wea. Rev.*, **134**, 272–292.
- Wood, V. T., and R. A. Brown, 1992: Effects on radar proximity on single-Doppler velocity signatures of axisymmetric rotation and divergence. *Mon. Wea. Rev.*, **120**, 2798–2807.
- , and —, 1997: Effects of radar sampling on single-Doppler velocity signatures of mesocyclones and tornadoes. *Wea. Forecasting*, **12**, 928–938.
- Wurman, J., and S. Gill, 2000: Finescale radar observations of the Dimmitt, Texas (2 June 1995), tornado. *Mon. Wea. Rev.*, **128**, 2135–2164.
- , and M. Randall, 2001: An inexpensive, mobile, rapid-scan radar. Preprints, 30th Int. Conf. on Radar Meteorology, Munich, Germany, Amer. Meteor. Soc., CD-ROM, P3.4.